Optical transitions of Er^{3+} ions in fluorozirconate glass

M. D. Shinn and W. A. Sibley
Physics Department, Oklahoma State University, Stillwater, Oklahoma 74078

M. G. Drexhage and R. N. Brown
Rome Air Development Center, Hanscom Air Force Base, Massachusetts 01731

(Received 27 January 1983)

Optical-absorption, -emission, and -excitation spectra are presented for Er^{3+} ions in fluorozirconate glass. Measured oscillator strengths of the transitions between J manifolds at 300 and 15 K are compared with calculated electric and magnetic dipole oscillator strengths. Radiative rates for five luminescing states were calculated. The nonradiative rates from these excited states were determined by calculating the difference between the measured rates and the calculated radiative rates. The low-temperature nonradiative rates are in agreement with the phenomenological energy-gap law followed by rare-earth ions in a number of crystals and glasses. The temperature dependence of the lifetimes was analyzed using the Huang-Rhys theory of multiphonon emission. Values for the $^4I_{11/2}$ radiative and nonradiative rates obtained by the above methods are compared with those obtained applying the method Flaherty and DiBartolo used to study MnF_2:Er^{3+}. The multiphonon emission rates in fluorozirconate glass are much lower than the rates for the same levels of Er^{3+} in oxide glasses. Measurements of the bandwidths of the ground and excited states of Er^{3+} and the nearly exponential decay of the emissions indicate a relatively narrow distribution of site symmetries compared to oxide glasses.

I. INTRODUCTION

Heavy-metal fluoride glasses are generating a great deal of interest because of their potential use in the growing laser and optical-fiber communications industries.[1–5] One promising candidate is fluorozirconate glass, which is highly transparent from 0.3 to 6.0 μm, relatively easy to prepare, and can be doped with rare-earth fluorides without the need of charge compensation.

The optical properties of Er^{3+} in various materials have been extensively studied.[6–10] The purpose of this paper is to present data on the optical properties of Er^{3+} in fluorozirconate glass. Broadband excitation is employed, resulting in optical properties which are the sum of the transitions of the individual ions in various sites within the glass. The radiative and nonradiative rates of the transitions receive special attention. The probability for magnetic dipole transitions can be readily calculated given the appropriate wave functions. The electric dipole transitions are forbidden within the $4f^{11}$ configuration of Er^{3+}, but forced electric dipole transitions occur due to admixing of odd-parity terms of higher-energy configurations into the $4f^{11}$ configuration, and by perturbations in this configuration by odd-order terms of the host's Stark field. Judd[11] and Ofelt[12] independently showed that by using several simplifying assumptions, the probabilities of forced electric dipole transitions can be expressed as the sum of a small number of phenomenological parameters. These parameters are determined by a best fit of calculated and observed oscillator strengths. The parameters may then be used to calculate the electric dipole contribution to the total spontaneous-emission probabilities. By subtracting the calculated radiative rates from the measured rates, the probability of nonradiative transitions can also be found. This method of determining radiative and nonradiative rates of rare-earth transitions has been used for solutions, crystals, and glasses.[8,13–19]

Other methods for calculating radiative and nonradiative rates have been developed. Flaherty and DiBartolo[20] formulated expressions for the nonradiative rate between two levels using the lifetimes and integrated intensities of these transitions at two different temperatures. The radiative rate of the higher energy level may then be determined. Huang and Rhys[21] developed a theory describing the temperature dependence of the nonradiative rate which is based on a single-configuration-coordinate model in which the parabolas representing the ground- and excited-state oscillators both have the same force constants, but whose minima are offset. Struck and

 ©1983 The American Physical Society

Fonger[22] present a more general treatment which places no constraints on force constants or offsets. They have also shown[23] that their treatment reduced to the Huang-Rhys expression if equal force constants are assumed, an assumption which should hold for Er^{3+} because the $4f$ electrons are well shielded by the $5s$ and $5p$ electrons.

II. THEORY

The theory and methods for calculating the probability of radiative transitions of rare-earth ions has been well described earlier[11–17,24–26]; thus only a short summary and the most essential formulas will be given. The free-ion states of a rare-earth ion are composed of linear combinations of Russell-Saunders states which are found by diagonalizing the combined electrostatic and spin-orbit energy matrices. The effect of the host's Stark field reduces the $(2J+1)$-fold degeneracy of the free-ion states and causes a small admixing of states. Because the effect of the field on the $4f^N$ configuration is small it is treated as a perturbation of the free-ion states. The calculated states have the configuration-interaction energy included in the matrix to be diagonalized. The necessary coupling coefficients are treated as parameters which are adjusted to obtain a best fit of the calculated J levels to those observed for the rare-earth ion in the host. The calculated states have the form

$$|f^n[\alpha SL]J\rangle = \sum_{\alpha,S,L} C_{\alpha SL}\,|f^N\alpha SLJ\rangle\ , \tag{1}$$

where the $C_{\alpha SL}$ are the coupling coefficients transforming the R-S states to intermediate-coupled states. The bracketed quantities indicate that the total angular momentum J is a good quantum number but the spin and orbital quantum numbers, S and L, respectively, are not. The symbol α includes all other quantum numbers needed to specify the states. Magnetic dipole and electric quadrupole transitions require no change in parity between states and thus can be allowed transitions, subject to selection rules, between states of a given configuration. The line strength for magnetic dipole (md) transitions between J manifolds is

$$S_{\rm md}(aJ;bJ') = \frac{e^2\hbar^2}{4m^2c^2}(\langle f^N[\alpha SL]J||\vec{\mathrm{L}}+2\vec{\mathrm{S}}||f^N[\alpha'S'L']J'\rangle)^2\ . \tag{2}$$

The probabilities for electric quadrupolar transitions of rare-earth ions have been found to be very much smaller[17,25] than dipolar transitions and are not considered in this work. The electric dipole (ed) line strengths are calculated in the Judd-Ofelt approach as the sum of intensity parameters Ω_t and doubly reduced matrix elements of tensor operators $U^{(t)}$ of rank t, with $t=2,4,6$ due to the selection rule $|\Delta J|\le 2l$ and $l=3$ for lanthanides, and is

$$S_{\rm ed}(aJ;bJ') = e^2 \sum_{t=2,4,6} \Omega_t(\langle f^N[\alpha SL]J||U^{(t)}||f^N[\alpha'S'L']J'\rangle)^2\ . \tag{3}$$

The intensity parameters Ω_t contain terms which are difficult to calculate. These include contributions from the crystal field, the interconfigurational radial integrals, and the average energy separation of the opposite parity configuration.

The oscillator strength of a transition of average frequency $\bar{\nu}$ from a level J to a level J' is

$$f(aJ;bJ') = \frac{8\pi^2 m\bar{\nu}}{3h(2J+1)e^2n^2} \times[\chi_{\rm ed}S_{\rm ed}(aJ;bJ') + \chi_{\rm md}S_{\rm md}(aJ;bJ')]\ , \tag{4}$$

where the χ terms correct for the effective field at a well-localized center in a medium of isotropic refractive index n and are given by $\chi_{\rm ed}=n(n^2+2)^2/9$ for electric dipole transitions and $\chi_{\rm md}=n^3$ for magnetic dipole transitions. In calculating the oscillator strength the selection rules for magnetic dipole transitions must be considered, i.e., $\Delta S=\Delta L=0$, $\Delta J=0,\pm1$ (but not $0\leftarrow$ or $0\rightarrow0$). First-principles calculations of the Ω_t parameters are hampered by the uncertainties which are inherent in the terms these parameters contain. The common way of determining the Ω_t parameters is to determine the oscillator strengths of the transitions by measurements of the integrated absorption coefficients. This relationship is

$$f = \frac{mc}{\pi e^2 N}\int \sigma(\nu)d\nu \tag{5}$$

and

$$\sigma(\nu) = \frac{\ln[I_0(\nu)/I(\nu)]}{t}\ , \tag{6}$$

where N is the number of ions per cm^3 and t is the

absorption path length. Through Eq. (5) the oscillator strengths of the various observed transitions may be used in Eq. (4). A least-squares-fitting approach may then be used to find the Ω_t parameters which give the best-fitted oscillator strengths.

The matrix elements of $\vec{L}+2\vec{S}$ and $U^{(t)}$ are calculated using formulas given elsewhere.[17,24] Since the free-ion eigenstates show only small changes with host, it has been found that the matrix elements of $U^{(t)}$ are essentially the same from host to host.[8,14,15,25] In this work the matrix elements calculated by Weber[17] for Er^{3+} in LaF_3 have been used. By using free-ion eigenstates, equal population in the Stark levels of the initial J state are assumed, a condition which is only approximately fulfilled at room temperature. It has been found that the addition of transitions to many different states tends to average the effects of unequal level populations.

The total spontaneous-emission probability is given by

$$A(aJ;bJ')=\frac{64\pi^4\bar{\nu}^3}{3(2J+1)hc^3}(\chi_{\rm ed}S_{\rm ed}+\chi_{\rm md}S_{\rm md}) , \tag{7}$$

which is related to the radiative lifetime τ of an excited state i by

$$\frac{1}{\tau_i}=\sum_j A(i,j) , \tag{8}$$

where the summation is over electric and magnetic dipole transitions to all terminal states j.

The multiphonon-emission rate of an excited state i to an adjacent, lower-lying state at some temperature in the absence of energy transfer is

$$W_{\rm NR}=\frac{1}{\tau_{\rm obs}}-\frac{1}{\tau_i} , \tag{9}$$

where $\tau_{\rm obs}$ is the observed lifetime of state i at that particular temperature and the subscript NR stands for nonradiative.

As stated earlier, several techniques exist for calculating the temperature dependence of $W_{\rm NR}$.[20–22,25,27] Huang and Rhys[21] developed a single–configuration-coordinate model where nonradiative transitions between levels occur with a single-phonon energy $\hbar\omega$. Their expression for the nonradiative rate is given by

$$W_{\rm NR}=N\exp\left[-S_0\frac{1+r}{1-r}\right]\times\sum_{j=0}^{\infty}\left[S_0\frac{r}{1-r}\right]^j\times\left[S_0\frac{1}{1-r}\right]^{p+j}\Big/ j!(p+j)! , \tag{10}$$

where N is a constant on the order of 10^{13} s^{-1}, p is the number of phonons required to span the energy gap between the two levels, and $r=\exp(-\hbar\omega/kT)$. The Huang-Rhys factor is $S_0=\Delta E/2\hbar\omega$, where ΔE is a measure of the relative offset between these levels.

Flaherty and DiBartolo[20] developed a method for calculating the nonradiative rate based on measurements of integrated emission intensities and lifetimes at different temperatures. If a fluorescent level B is excited entirely through nonradiative transitions from a higher-lying fluorescent level A, the nonradiative rate W_{AB} is given at temperatures T_1 and T_2 by

$$W_{AB}(T_1)=\frac{1}{\tau_A(T_1)}-\frac{1}{\tau_A(T_2)}\times\left[1-\frac{\tau_B(T_1)}{\tau_B(T_2)}\frac{I_A(T_1)}{I_B(T_1)}\frac{I_B(T_2)}{I_A(T_2)}\right]^{-1} \tag{11}$$

and

$$W_{AB}(T_2)=\frac{1}{\tau_A(T_2)}-\frac{1}{\tau_A(T_1)}\times\left[1-\frac{\tau_B(T_2)}{\tau_B(T_1)}\frac{I_A(T_2)}{I_B(T_2)}\frac{I_B(T_1)}{I_A(T_1)}\right]^{-1} , \tag{12}$$

where τ_A and τ_B are the measured lifetimes and I_A and I_B are the measured integrated intensities of levels A and B, respectively. The radiative rate of level A may be found by substituting W_{AB} from Eq. (11) or (12) and the value of τ_A, at the same temperature, in Eq. (9). This technique requires only relative measurements of intensities; no absolute intensity measurements or calibration of the detection system is required.

In principle, it is possible to use time-dependent perturbation theory to calculate the multiphonon-emission rate. Uncertainties in determining some of the parameters limit the theory to order-of-magnitude estimates.[25] A phenomenological model of multiphonon emission based on this perturbation-theory expression was developed by Riseberg and Moos[27] and applied by several investigators.[8,18,20,25,26] The model assumes that only phonons of a single frequency are active in the nonradiative transition. The expression for the temperature dependence of the nonradiative rate is

TABLE I. Compositions and properties of some heavy-metal fluoride glasses.

Glass	Composition (mol %) ZrF_4	HfF_4	BaF_2	LaF_3	ThF_4	AlF_3	ErF_3	T_g (°C)	T_x (°C)	Density (g/cm^3)
ZBT[a]	58		33		9			315	394	4.86
ZBL[b]	60		35	5						
HBT[a]		58	33		9			319	396	6.19
HBL[a]		58	33	9				332	415	5.56
ZBLA: 0.5% Er	57		35.5	3		4	0.5	~310	~390	4.61
ZBLA: 2.0% Er	57		34	3		4	2	~310	~390	4.61

[a]Reference 29.
[b]Reference 30.

$$W_{NR}(T)=W_{NR}(0)\left[\frac{\exp(\hbar\omega/kT)}{\exp(\hbar\omega/kT)-1}\right]^{p}, \quad (13)$$

where p is the number of phonons emitted in the transition and $W_{NR}(0)$ is the low-temperature multiphonon-emission rate. This expression has been found to account fairly well for the temperature dependence of the nonradiative rate, as determined by using Eq. (9) at different temperatures. It has been noted that the single-phonon models work best when the highest-energy phonon mode is used, i.e., the transition occurs in the lowest order of p possible, so long as energy is conserved.[17,18,20,22,25–27] The only exceptions to this trend occur when the highest-energy phonons are very weak compared to the rest of the phonon spectrum. In this case the more dominant, lower-energy phonon modes appear to be responsible for the nonradiative transitions.[8,25]

III. EXPERIMENTAL METHODS

The samples used in this study were prepared using methods described earlier.[3,28,29] Two samples were prepared, with 2.0 at. % Er^{3+} and 0.5 at. % Er^{3+} added to the melt. The compositions of several common heavy-metal fluoride glasses and some of their properties are given in Table I.[29,30] The glass transition temperature is given by T_g and the onset of crystallization by T_x. The addition of AlF_3 to the samples extends the range of compositions under which glass formation is possible.[28] Measurements of the final compositions have always indicated that they are within ~1–2 mol % of the starting composition.[28] The glasses will be identified based on their compositions, as indicated in Table I.

For low-temperature measurements, a Sulfrian helium cryostat, or a CTI Cryodyne Cryocooler Model 21SC with a resistence heater which allows temperature control within ±1 K over the range 14–300 K, was utilized. Above room temperature the sample was enclosed in a copper holder with small windows for the excitation light and the fluorescence. In this case a copper-Constantan thermocouple was mounted directly on the sample to measure the temperature. The temperature above room temperature was controlled within ±5 K with a resistance heater.

Emission- and excitation-spectra measurements were made by exciting the samples with light from a 75-W xenon-arc lamp which had been passed through a 0.22-m Spex monochromator. The fluorescence was focused into a 0.8-m Spex monochromator and mirrors were used to route the light emerging from the exit slit to the appropriate detector. These detectors were a cooled RCA C31034 photomultiplier tube (PMT) for the visible, a cooled RCA 7102 PMT for the near infrared, and a cooled Optoelectronics OTC-22-53 PbS cell for the infrared. The signal from the detector was preamplified and passed to a lock-in amplifier that was synchronized with a variable-speed light chopper in the excitation beam. The output of the lock-in amplifier may be displayed on an X-Y recorder or stored on tape by a Hewlett-Packard HP-85 minicomputer. Lifetime measurements were made utilizing a Biomation 610B transient recorder and a Nicholet 1070 signal averager. This system allowed lifetimes as short as 10 μs to be measured. For all lifetime measurements the fluorescing level was directly excited. This is especially important when nonradiative rates are slow. Optical-absorption measurements were made using a Cary 14 spectrophotometer with either (0–0.1)- or (0–1.0)-OD (optical density) slidewires, or a Perkin-Elmer 330 spectrophotometer. At all times the spectral resolution was much greater than the observed linewidths. Integrated intensities were calculated by numerical integration. The intensity of the exciting light at the sample position was measured with a Photo Research 310 photometer-radiometer and the excitation spectra are corrected accordingly, except where noted.

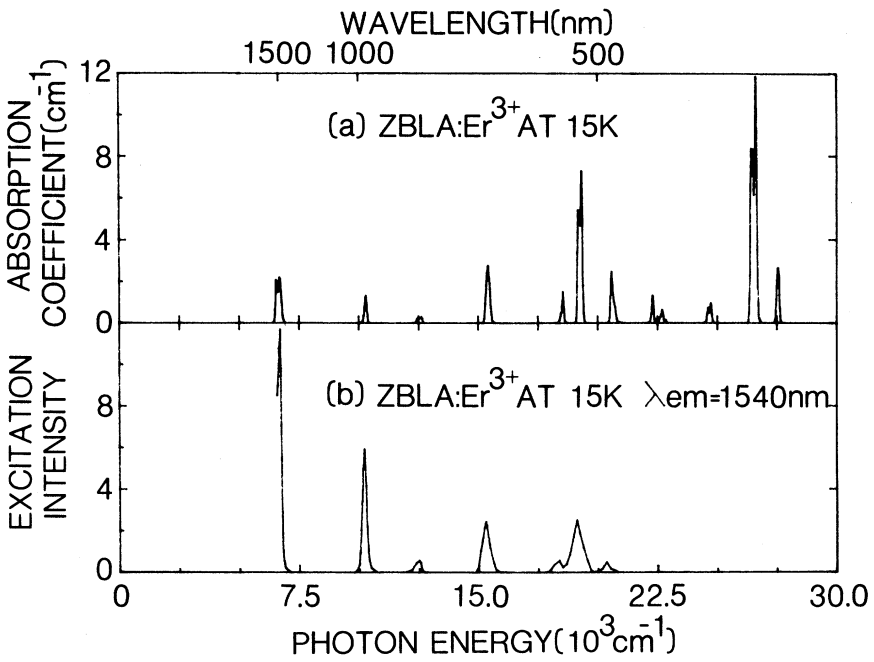

FIG. 1. (a) Absorption spectrum of Er^{3+} in ZBLA. (b) ${}^4I_{13/2} \rightarrow {}^4I_{15/2}$ excitation spectrum of Er^{3+} in ZBLA.

IV. EXPERIMENTAL RESULTS

The absorption spectrum of the 2.0 at. % Er^{3+} sample is shown in Fig. 1(a), with the ${}^4I_{13/2} \rightarrow {}^4I_{15/2}$ excitation spectrum shown in Fig. 1(b) for comparison. Excitation bands of higher energy than those shown were observed; however, their low intensity with respect to the noise made it impossible to accurately correct their intensities. The absorption coefficients of the 0.5 at. % Er^{3+} sample were only one-fourth as large as the absorption coefficients of the 2.0 at. % Er^{3+} sample except for the band at 12 500

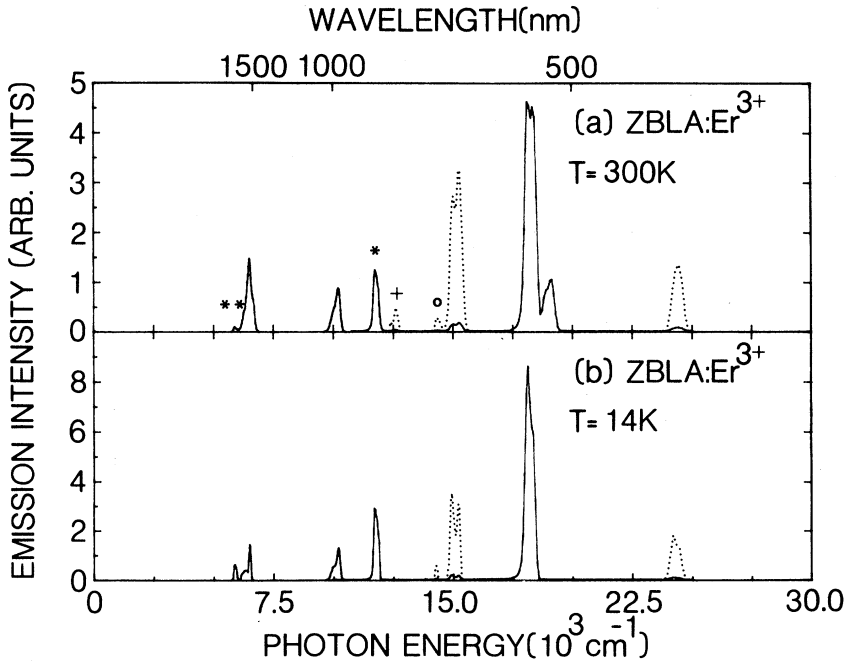

FIG. 2. Emission spectrum of Er^{3+} in ZBLA at (a) 300 K and (b) 14 K. The symbols above the bands are explained in the text. Bands plotted as dotted lines have had their intensities increased by a factor of 20.

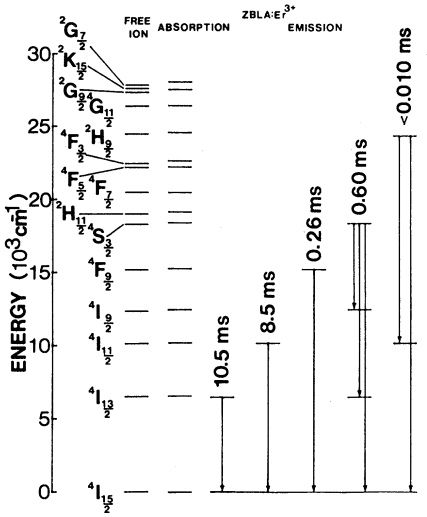

FIG. 3. Energy-level diagram of Er^{3+} as a free ion (Ref. 6), and for the present work. Also indicated are the lifetimes (in ms) of the fluorescent levels at 14 K.

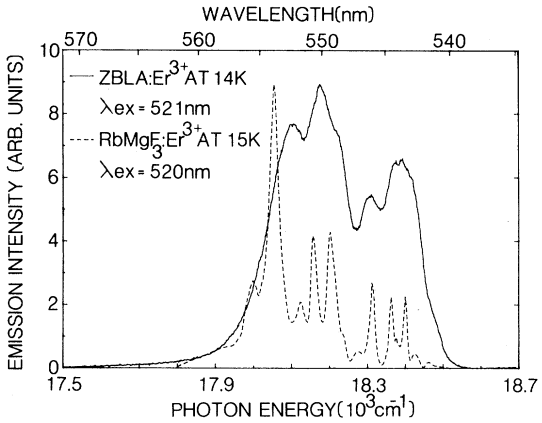

FIG. 4. $^4S_{3/2} \rightarrow {}^4I_{15/2}$ emission spectrum of Er^{3+} in ZBLA (solid line) and $RbMgF_3$ (dotted line).

cm^{-1} (800 nm) which was more intense. This sample's absorption spectrum also contained weak bands at $\sim 13\,514$ cm^{-1} (740 nm) and $\sim 17\,361$ cm^{-1} (576 nm). Comparison with earlier work on Nd^{3+} in ZBL glass[28] shows absorption bands at the same three positions. The concentration of Nd^{3+} in our sample was determined to be about 0.005 at. % (8.2×10^{17} cm^{-3}) by comparing the intensities of the Nd^{3+} bands with those of ZBL:Nd^{3+}.[28] The emission spectra of Er^{3+} at 300 and 14 K are shown in Figs. 2(a) and 2(b), respectively. In these figures the line marked with an asterisk is the transition $^4S_{3/2} \rightarrow {}^4I_{13/2}$, the line marked with a plus is the transition $^2H_{11/2} \rightarrow {}^4I_{13/2}$, the line marked with a circle is the transition $^2H_{9/2} \rightarrow {}^4I_{11/2}$, and the line marked with a double asterisk is the transition $^4S_{3/2} \rightarrow {}^4I_{9/2}$. All other transitions are from excited states to the ground state. An energy-level diagram for ZBLA:Er, using the data presented in Figs. 1 and 2, is shown in Fig 3. Included are the energy levels of the free ion,[6] and the measured lifetimes at 14 K.

In an amorphous host an impurity ion does not occupy any one site symmetry, but instead occupies a large number of different sites. This results in inhomogeneous broadening of the emission and absorption lines. The high-resolution emission spectrum of the $^4S_{3/2} \rightarrow {}^4I_{15/2}$ transition (solid line), which shows the extent of the ground-state splitting and inhomogeneous broadening, is presented in Fig. 4. Superimposed on this spectrum is the same emission of Er^{3+} from one site in $RbMgF_3$.[10] It is ap-

TABLE II. Measured oscillator strengths of Er^{3+} in various hosts. All transitions are from the $^4I_{15/2}$ level to the levels indicated.

		Oscillator strength ($\times 10^8$)					
Level		$YA1O_3^8$ 300 K	$Y_2O_3^{13}$ 300 K	PZGL[a] 300 K	ZBLA: 0.5% Er 300 K	ZBLA: 2.0% Er 300 K	2.0% Er 15 K
$^4I_{13/2}$	magnetic dipole	59	52	201	46	46	46
	electric dipole	68	73		125	103	131
$^4I_{11/2}$		31	34	67	49	56	52
$^4I_{9/2}$		25	31	32	25	20	21
$^4F_{9/2}$		115	173	176	180	164	175
$^4S_{3/2}$		41	34	41	33	39	47
$^2H_{11/2}$		243	1103	278	436	394	452
$^4F_{7/2}$		112	113	125	138	141	128
$^4F_{5/2}$		60	40	63	61	71	47
$^4F_{3/2}$				35			32
$^2H_{9/2}$		42	61	56	47	47	54
$^4G_{11/2}$		431	2055	581	778	841	875

[a]Reference 15. PZGL is a glass composed of (in mol %) 46 PbF_2:22 ZnF_2:30 GaF_2:2 LaF_3.

TABLE III. Calculated oscillator strengths of Er^{3+} in ZBLA glass. All transitions are from the $^4I_{15/2}$ level to the levels indicated.

Level	Oscillator strength ($\times 10^8$) Wavelength (nm)	Oscillator strength	Residual
$^4I_{13/2}$	1516	97.6	28
$^4I_{11/2}$	976	42.2	7
$^4I_{9/2}$	800	23.9	−1
$^4F_{9/2}$	653	173.7	6
$^4S_{3/2}$	542	37.4	−5
$^2H_{11/2}$	521	432.0	4
$^4F_{7/2}$	487	153.2	−15
$^4F_{5/2}, ^4F_{3/2}$	448	68.4	−7
$^2H_{9/2}$	406	62.2	−15
$^4G_{11/2}$	378	780.4	−2

parent that the ground-state splitting of Er^{3+} in this glass is no broader than that in $RbMgF_3$ crystals. The data in Fig. 4 suggest that the types of site symmetries in ZBLA are fewer in number than in oxide glasses. This has been previously explained as being due to Er^{3+} substituting only as a network former, unlike the case for oxide glasses, where Er^{3+} may substitute for both network formers and modifiers.[15,28]

The oscillator strengths of the absorption transitions were calculated using Eq. (5). All transitions were assumed to be electric dipole in nature, except for the $^4I_{15/2} \rightarrow {}^4I_{13/2}$ transition, which has a substantial magnetic dipole component. The values for both glass samples are presented in Table II. Values for Er^{3+} in several other hosts are shown for comparison. The value of N, the concentration, was taken to be equal to the concentration in the starting mixture. This has been found to be true for previous rare-earth dopings of fluoride glasses.[28] The value of the $^4I_{9/2}$ oscillator strength for the 0.5 at.% Er^{3+} sample was estimated by integrating the entire band and subtracting the contribution due to 0.005 at.% Nd^{3+}. The index of refraction was measured at two wavelengths and the indices of refraction at all other wavelengths were calculated using Cauchy's equation $n = A + B/\lambda^2$, with $A = 1.505\,83$ and $B = 3478.14$ nm^2. The average frequencies of the transitions were taken to be the centers of gravity of the absorption bands. These values were substituted into Eqs. (3) and (4) and the Judd-Ofelt parameters adjusted to give the best least-squares fit to the measured oscillator strengths. For the $^4I_{13/2}$ absorption, the magnetic dipole oscillator strength was calculated using Eqs. (2) and (4) and subtracted from the measured oscillator strength to give the electric dipole oscillator strength. The Judd-Ofelt parameters are $\Omega_2 = 2.54 \times 10^{-20}$ cm^2, $\Omega_4 = 1.39 \times 10^{-20}$ cm^2, and $\Omega_6 = 9.65 \times 10^{-21}$ cm^2. The calculated oscillator strengths are given in Table III. A measure of the quality of the fit is given by the rms deviation between the measured and calculated oscillator strengths, as calculated from the relationship

$$\delta_{\text{rms}} = \left[\frac{\text{sum of squares of deviations}}{\text{number of transitions} - \text{number of parameters}} \right]^{1/2} . \tag{14}$$

The rms deviation for the 0.5 at.% Er^{3+} sample is 0.14×10^{-6}, which is comparable to the rms deviations found by applying the Judd-Ofelt theory to Er^{3+} in other systems.[8,12,14,28] The radiative lifetimes of the excited states can be calculated from Eqs. (7) and (8). While forced electric dipole transitions comprise most of the spontaneous-emission probabilities of any level, the magnetic dipole emis-

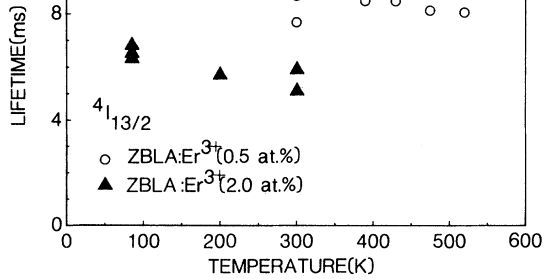

FIG. 5. Temperature dependence of the $^4I_{13/2}$ emission lifetimes.

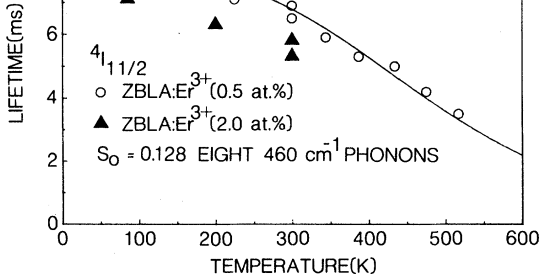

FIG. 6. Temperature dependence of the $^4I_{11/2}$ emission lifetimes.

TABLE IV. Predicted spontaneous-emission probabilities of Er^{3+} in ZBLA glass.

Transition	Average frequency (cm^{-1})	P_{ed} (s^{-1})	P_{md} (s^{-1})	τ_R (ms)
$^4I_{13/2}\rightarrow{}^4I_{15/2}$	6596	73.5	34.7	9.2
$^4I_{11/2}\rightarrow{}^4I_{15/2}$	10246	89.9		9.2
$^4I_{13/2}$	3650	10.9	7.7	
$^4I_{9/2}\rightarrow{}^4I_{15/2}$	12500	90.6		8.3
$^4I_{13/2}$	5904	28.9		
$^4I_{11/2}$	2254		1.1	
$^4F_{9/2}\rightarrow{}^4I_{15/2}$	15314	994.4		0.92
$^4I_{13/2}$	8718	48.6		
$^4I_{11/2}$	5068	40.9		
$^4I_{9/2}$	2814	1.3		
$^4S_{3/2}\rightarrow{}^4I_{15/2}$	18450	782.3		0.86
$^4I_{13/2}$	11854	316.1		
$^4I_{11/2}$	8204	25.4		
$^4I_{9/2}$	5950	41.5		
$^2H_{11/2}\rightarrow{}^4I_{15/2}$	19194	3264.4		0.31
$^2H_{9/2}\rightarrow{}^4I_{15/2}$	24631	937.6		0.44
$^4I_{13/2}$	18034	1010.1		
$^4I_{11/2}$	14385	302.4		
$^4I_{9/2}$	12131	11.9		
$^4F_{9/2}$	9317	23.1		

sion probabilities were also calculated for the $^4I_{13/2}\rightarrow{}^4I_{15/2}$, $^4I_{11/2}\rightarrow{}^4I_{13/2}$, and $^4I_{9/2}\rightarrow{}^4I_{11/2}$ transitions. The values obtained are shown in Table IV.

The temperature dependences of the lifetimes of both samples are shown in Figs. 5–8. Although fluorescence was detected from the $^2H_{9/2}$ level, the lifetime was faster than could be measured with our system. The errors in these measurements are estimated to be $\sim 5\%$. The decays of the $^4I_{13/2}$ and $^4I_{11/2}$ levels could be fitted to a single exponential while the $^4S_{3/2}$ and $^4F_{9/2}$ levels were very nearly single exponential, with a ratio between the first and third e-folding times of the latter two levels of $\gtrsim 85\%$. For these levels the first e-folding times were used as the values of the lifetimes.

Comparison of Fig. 2(a) with Fig 2(b) shows that the emission at 19120 cm^{-1} (523 nm) decreases in intensity as the temperature is lowered. The energy of the emission and its excitation spectrum identify this emission as the $^2H_{11/2}\rightarrow{}^4I_{15/2}$ transition, which is populated thermally by the $^4S_{3/2}$ level. This behavior has been observed previously.[14,17] An analysis based on a simple three-level system comprised of the $^2H_{11/2}$ (level 3), $^4S_{3/2}$ (level 2), and $^4I_{15/2}$ levels predicts that the thermalization can be expressed by the following equation:

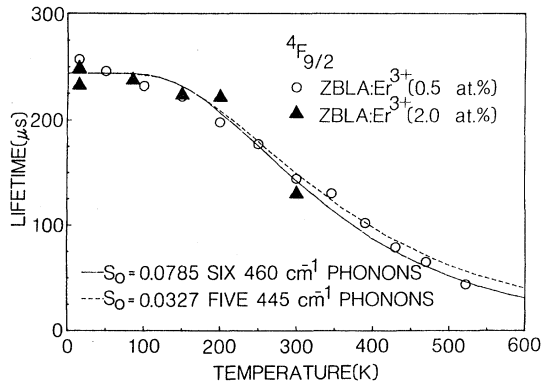

FIG. 7. Temperature dependence of the $^4F_{9/2}$ emission lifetimes.

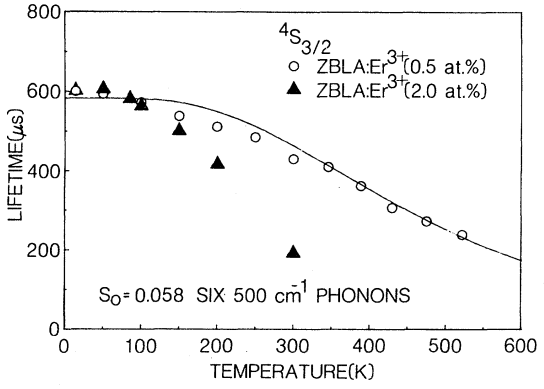

FIG. 8. Temperature dependence of the $^4S_{3/2}$ emission lifetimes.

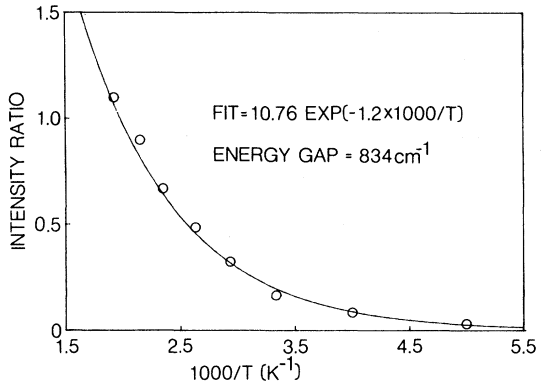

FIG. 9. Ratio of the integrated intensities of the $^2H_{11/2}\rightarrow{}^4I_{15/2}$ and $^4S_{3/2}\rightarrow{}^4I_{15/2}$ emissions as a function of $1000/T$.

$$\frac{I_3}{I_2}=\frac{c_3(\nu)p_3^r g_3 h\nu_3}{c_2(\nu)p_2^r g_2 h\nu_2}\exp\left[-\frac{E_{32}}{kT}\right], \tag{15}$$

where g_3,g_2 are the degeneracies $(2J+1)$, and p_3^r and p_2^r are the total spontaneous-emission rates of the $^2H_{11/2}$ and $^4S_{3/2}$ levels, respectively. The response of the detection system in the frequency range of the $^2H_{11/2}$ and $^4S_{3/2}$ levels is given by $c_3(\nu)$ and $c_2(\nu)$, respectively. The photon energies of the two bands are so similar that they are considered equal. This relation was checked by recording the two emission spectra at various temperatures and plotting the ratio of the intensities versus $1000/T$ as shown in Fig. 9. The line is a least-squares fit to the data, and it can be seen that a good fit to Eq. (15) is obtained. The value of the preexponential factor can be estimated from the product of the ratio of the degeneracies (3), the ratio of the radiative rates (~ 2.8), and the ratios of the detection-system correction factors (~ 1.5) to be about 13; this agrees well with the fitted value of 10.76. The value of the energy gap between the two levels, E_{32}, was found to be ~ 830 cm^{-1}. This is a reasonable value if one considers the transition to occur from the relaxed excited state of the $^4S_{3/2}$ level to the $^2H_{11/2}$ level. Previous investigators[14,15] have neglected the difference in the Stoke's shifts of the two levels and calculated E_{32} from absorption data alone.

It was mentioned earlier that the 0.5 at. % Er^{3+} sample also contained 0.005 at. % Nd^{3+}. The emission spectrum of the Nd^{3+} ions at 300 K is shown in Fig. 10. The emission at 11 521 cm^{-1} (868 nm) is the $^4F_{3/2}\rightarrow{}^4I_{9/2}$ transition. The very weak emission at 12 469 cm^{-1} (802 nm) is believed to be the $^4F_{5/2}$ or $^2H_{9/2}\rightarrow{}^4I_{9/2}$ emission with the excitation being provided due to thermal population from the $^4F_{3/2}$ level. The identification of this emission is based on several observations: the excitation spectrum is that expected for the $^4F_{5/2},^2H_{9/2}$ levels, the lifetime is the same as the $^4F_{3/2}$ lifetime, and the emission decreases in intensity as the temperature is lowered. The thermalization is extremely weak, as is evidenced by the lack of any effect on the $^4F_{3/2}$ lifetime, which was 444 μs at 15 and 300 K. This was the same value found, within experimental error, in ZBL:Nd.[28] Figure 11 shows the Nd^{3+} $^4F_{3/2}$ excitation spectrum (solid line). The $^4F_{3/2}$ emission is in the same spectral range as the Er^{3+} $^4S_{3/2}\rightarrow{}^4I_{13/2}$

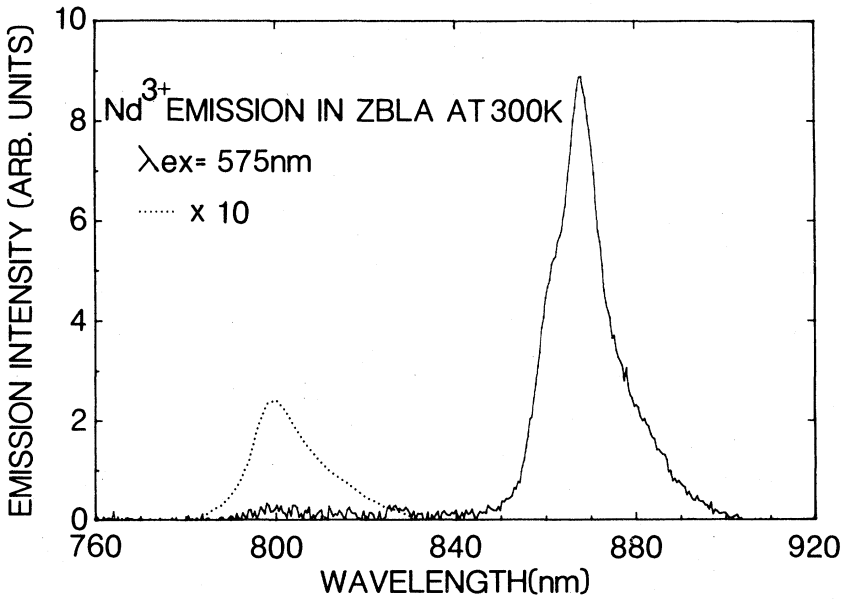

FIG. 10. Emission spectrum of Nd^{3+} in ZBLA at 300 K.

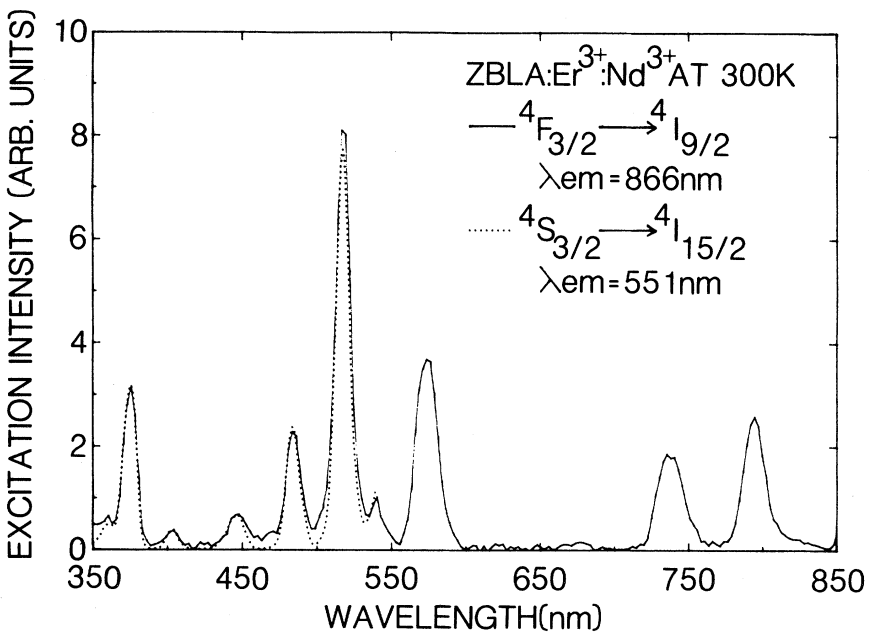

FIG. 11. Uncorrected $^4F_{3/2} \rightarrow {}^4I_{9/2}$ excitation spectrum of Nd^{3+} (solid line) and the $^4S_{3/2} \rightarrow {}^4I_{15/2}$ excitation spectrum of Er^{3+} (dotted line) in ZBLA at 300 K.

emission, which in this sample is about 10 times more intense. Consequently, Er^{3+} bands are present in the Nd^{3+} excitation spectrum. To check if these Er^{3+} excitation bands are actually part of the Nd^{3+} excitation spectrum the $^4S_{3/2} \rightarrow {}^4I_{15/2}$ excitation spectrum is also portrayed in Fig. 11 (dotted line), and is scaled to have the same intensity at the $^4G_{11/2}$ level (378 nm). In Fig. 11 all other Er^{3+} bands have the same peak intensity, except the $^2H_{11/2}$ excitation peak at 521 nm. This discrepancy is due to excitation of the Nd^{3+} ions from the $^4G_{7/2}$, $^4G_{9/2}$, and $^2K_{13/2}$ levels, which are at 521 nm in ZBL glass.[28] Inspection of Fig. 11 shows that no bands in the Nd^{3+} excitation spectrum for $\lambda < 550$ nm exist which are not due to Nd^{3+}.

V. DISCUSSION

A. Multiphonon emission

Previous studies have indicated that nonradiative relaxation of excited states of rare-earth ions in solids is through the emission of phonons.[7,8,18,19,25,26,31,32] This assumes that nonradiative effects due to ion-ion cooperation are negligible. These investigations have also found that the rates of multiphonon emission are sensitive to the number of phonons emitted in the transition. The lifetime of an excited state was found to be temperature independent (no multiphonon emission) if approximately ten or more phonons were required to make the transition between it and the next lowest-lying level. Conversely, the luminescence was totally quenched if fewer than four phonons were required for the transition. Levels with energy gaps between these two extremes have temperature-dependent lifetimes. Since the energy gaps change only negligibly with host for the trivalent lanthanides, the factor influencing the multiphonon-emission rate is the energy of the phonons involved in the transition. The phonon density of states can be partially determined from infrared reflectivity and Raman data. Infrared reflectivity measurements of ZBL glass show bands at ~ 500 and ~ 270 cm^{-1}.[30]

The observed multiphonon-emission rates for the $^4S_{3/2}$, $^4F_{9/2}$, and $^4I_{11/2}$ levels in the 0.5 at.% Er^{3+} sample were calculated from Eq. (9) using the radiative rates predicted by the Judd-Ofelt theory and the measured lifetimes. To apply the Huang-Rhys theory to these values the phonon energy, the number of phonons required to span the energy gap, and the Huang-Rhys factor S_0 are needed. The number of phonons may be calculated readily from the relation $p = E/\hbar\omega$, where E is the value of the energy gap. Owing to inhomogeneous broadening, the Huang-Rhys factors and energy gaps are not definitely known experimentally; however, it is possible to establish reasonable limits for these parameters from the absorption and emission spectra. Initial values for these parameters were substituted into Eq. (10) and the values of S_0 and $\hbar\omega$ were adjusted to give the best fit to the observed rates. These

Huang-Rhys-predicted multiphonon-emission rates and the radiative rates were then substituted back into Eq. (9) to predict the measured lifetimes. These predicted lifetimes are shown as solid lines in Figs. 6–8. It should be noted that the radiative rate of the $^4S_{3/2}$ level cannot be assumed temperature independent, due to thermalization with the $^2H_{11/2}$ level. The effective radiative-emission probability for the two levels may be calculated from the formula[15]

$$A_{\text{eff}}=\frac{12A(^2H_{11/2})\exp(-\Delta E/kT)+4A(^4S_{3/2})}{12\exp(-\Delta E/kT)+4} \tag{16}$$

using the values of $A(^2H_{11/2})$ and $A(^4S_{3/2})$ given in Table IV and the value of $\Delta E=830$ cm^{-1} obtained from the data presented in Fig. 9. This change in the radiative rate with temperature was taken into account when the observed multiphonon-emission rate for the $^4S_{3/2}$ level was calculated. The Huang-Rhys theory predicts such a low multiphonon-emission rate ($\ll 10^{-10}$s^{-1}) at all temperatures for the $^4I_{13/2}$ level that the lifetime should be temperature independent. The line drawn in Fig. 5 is thus the lifetime predicted by the Judd-Ofelt theory. The best fits were found using phonon energies in the range of 460–500 cm^{-1}. This value is consistent with the reflectivity data.[30] In all cases the calculated energy gaps and Huang-Rhys factors were within the limits imposed by the experimental data. The data in Figs. 6–8 indicate that the Huang-Rhys theory fairly accurately predicts the temperature dependence of the lifetimes of the $^4I_{11/2}$, $^4F_{9/2}$, and $^4S_{3/2}$ levels. From Fig. 5 it can be seen that, while the Judd-Ofelt, Huang-Rhys theoretical line is always within 10% of the measured values, these values show a slowly decreasing trend with increasing temperature. Several possibilities for explaining this behavior will be presented later.

A semilogarithm graph of the observed low-temperature multiphonon-emission rates versus the energy gap to the next lowest level is illustrated in Fig. 12. (Also plotted are the fitted rates and energy gaps.) It can be seen that an exponential dependence of the multiphonon-emission rate on energy gap is obeyed. This empirical "energy-gap law" was first noted during studies on multiphonon emission in crystals,[8,17,20,25,27] and later in glasses.[18,19,26] This relationship is expressed through the formula

$$W_{\text{NR}}=C\exp(-\alpha\Delta E)\,, \tag{17}$$

where C and α are positive constants characteristic of the host. It has been observed that once these parameters are determined, the nonradiative rate can be calculated through Eq. (17) (within a factor of 2)

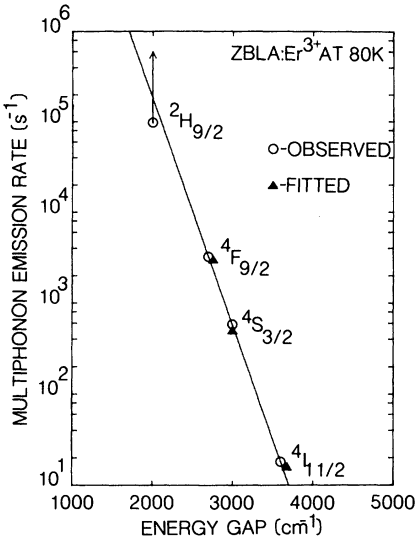

FIG. 12. Multiphonon emission rates of 0.5 at. % Er^{3+} in ZBLA at 80 K as a function of the energy gap to the next-lower level.

for any lanthanide ion in this host.[25] However, this expression is limited by uncertainties in determining the nonradiative rates for large and very small (one- or two-phonon process) energy gaps. A least-squares fit of the observed data to Eq. (17) with $C=1.88\times10^{10}$ s^{-1} and $\alpha=5.77\times10^{-3}$ cm is portrayed in Fig. 12. The lower bound for the multiphonon-emission rate of the $^2H_{9/2}$ level is also shown.

In the past the multiphonon-emission rate has been plotted versus the number of phonons p involved in the transition. Recently Fonger and Struck[23] proposed that the exponential dependence on p be replaced at low temperatures by the equation

$$W_{\text{NR}}(0)=N\exp(-S_0)S_0^p/p!\,, \tag{18}$$

which is the first term of Eq. (10) with $r=0$, valid for $S_0\ll1$. They attempted to fit experimental results with Eq. (18) using a fixed value of S_0; however, their predicted dependence of W_{NR} on p for reasonable values of S_0 and N was steeper than exhibited experimentally. The data in Fig. 12 show that when S_0 is allowed to vary slightly, the exponential trend of the data is reproduced.

It should be noted that in using the Huang-Rhys theory to fit the temperature dependences of the $^4S_{3/2}$ and $^4F_{9/2}$ lifetimes, the same number of phonons, six, was used. A Huang-Rhys fit for the $^4F_{9/2}$ level, using five phonons, is also shown in Fig. 7. The best fit used phonon energies of 445 cm^{-1}, requiring an energy gap smaller than measured. The value of S_0 was also smaller than the lower limit inferred from the data. The only major difference in

fitting the data in Fig. 7 and 8 was the value of S_0, yet it adequately accounted for the difference in the low-temperature multiphonon-emission rates for the two levels. Only recently has the influence of S_0 on W_{NR} been discussed for rare-earth ions, while it has long been recognized for transition-metal ions.[22,23]

It is also possible to use the single-phonon model [Eq. (13)] to fit the temperature dependence of multiphonon-emission rates. In all cases the single-phonon model's values at low temperatures were almost identical to the values predicted by the Huang-Rhys theory, and tended toward higher values for temperatures above ~ 200 K. However, even at the highest temperature (520 K) the single-phonon model's value is greater by only 6%. While ease of computation and success in predicting the behavior of the multiphonon-emission rate make the single-phonon model useful, its simplicity is also a liability. The low-temperature multiphonon rate is determined by the parameter $W_{NR}(0)$, which is found using Eq. (9). There is no way, using this model, to know if the value obtained is reasonable. The Huang-Rhys theory provides information to check the plausibility of the values of the multiphonon-emission rate, with only slightly more difficulty in performing the computations.

Thus far all our calculations involving the Huang-Rhys theory have assumed $N = 1 \times 10^{13}$ s^{-1} in Eq. (10). This value is in agreement with earlier estimates.[22,31] Inspection of Eq. (10) indicates that N can be varied less than an order of magnitude from this value without affecting the value of S_0 to such an extent that the fitted values fall outside the experimentally determined limits. Within these limits equally good fits may be obtained, with the S_0 values increasing when N is decreased, and vice versa.

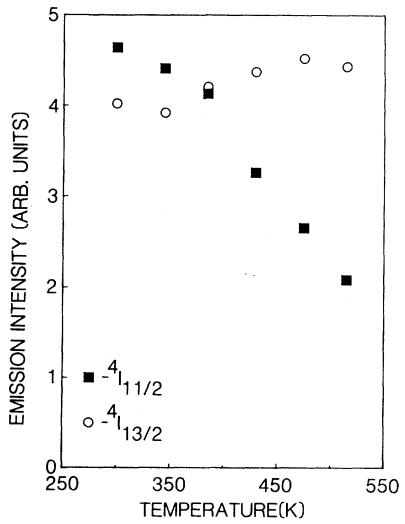

FIG. 13. Temperature dependence of the integrated intensities of the $^4I_{11/2} \rightarrow {}^4I_{15/2}$ and $^4I_{13/2} \rightarrow {}^4I_{15/2}$ emissions.

A method used by Flaherty and DiBartolo[20] for the calculation of radiative and nonradiative rates was discussed earlier. Since application of this method is relatively straightforward, with no need for absolute calibration of the detection system, it was used to calculate the radiative rate for the $^4I_{11/2}$ level. This level was chosen because the three-level system comprised of the $^4I_{11/2}$, $^4I_{13/2}$, and $^4I_{15/2}$ levels best fits the theoretical system considered by Flaherty and DiBartolo.[20] The 0.5 at. % Er^{3+} sample was used for all measurements. The $^4F_{9/2}$ level was used as the excitation level because of its relatively high oscillator strength and the low probability of level bypassing through radiative transitions to the $^4I_{11/2}$ and $^4I_{13/2}$ levels. The change in the integrated intensities of the $^4I_{11/2}$ and $^4I_{13/2}$ levels with temperature is shown in Fig. 13. The low signal-to-noise ratio of the $^4I_{13/2}$ data places large error bars ($\sim 10\%$) on the intensity values shown. The lifetimes of the two levels were taken from the data in Figs. 5 and 6. Substitution of these values into Eqs. (11) and (9) resulted in a mean calculated rate of 92 s^{-1} (10.8 ms) with a standard deviation of 27 s^{-1}. An attempt to fit the temperature dependence of the multiphonon-emission rate using this value of the radiative rate required seven 525-cm^{-1} phonons. This phonon energy is too high to provide a good fit to the temperature dependences of the $^4S_{3/2}$ and $^4F_{9/2}$ levels. It should be noted that for two sets of temperatures (300—345 and 300—385 K) the calculated multiphonon-emission rates were larger than the measured rates and had to be excluded. Closer analysis of the calculated rates showed that they did not lie about the mean but instead were in two groups. The lower-rate group corresponded to anamolous behavior in the $^4I_{13/2}$ intensities, such as the aforementioned results with the 300- and 345-K data points. Taking the higher-rate group as more accurate, the calculated radiative rate is 116.5 s^{-1} (8.6 ms) with a standard deviation of 20 s^{-1}, a value quite close to the value of 9.2 ms calculated using the Judd-Ofelt theory. On the basis of these analyses it appears that with accurate intensity and lifetime measurements the Flaherty-DiBartolo method can yield results as accurate as those provided by the Judd-Ofelt theory.

B. Energy transfer

Energy transfer occurs in many materials when rare-earth concentrations are as high as 2 at. %. In fact, previous investigations on ion-ion cooperative effects in crystals and glasses have shown that such effects occur for concentrations of about 1 at. % or

greater.[7,28,33] The data shown in Figs. 5–8 suggests that Er^{3+} ions in ZBLA glass exhibit energy transfer. The lifetimes of the fluorescent levels for both the 2 and 0.5 at. % samples are essentially the same at 15 K but the lifetimes of the 2.0 at. % sample decrease markedly in most cases as the temperature is raised. For the 0.5 at. % Er^{3+} sample, the situation is not so clear. The same investigations indicate negligible energy-transfer effects at this concentration. However, the lifetime of the $^4I_{13/2}$ level for this sample (Fig. 5) does have a temperature dependence even though the Huang-Rhys and single-phonon models predict there should be no such dependence. It is well established that with a given J manifold, differences in oscillator strengths, and hence radiative rates, are different for sublevels within a J manifold. It is possible that the temperature dependence of the $^4I_{13/2}$ level in the 0.5 at. % sample is due to thermalization of higher-lying sublevels in the J manifold with faster radiative rates. The appearance of a band at 6623 cm^{-1} (1510 nm) as the sample is warmed above 15 K supports this possibility. This type of thermalization would also explain a trend in the other lifetime data, where the measured lifetimes decrease somewhat faster than the predicted lifetimes in the temperature range from about 100 to 300 K.

The possibility of energy transfer between Nd^{3+} and Er^{3+} in the 0.5 at. % Er^{3+} sample also must be considered since the Er^{3+} $^2H_{11/2}$ level and the Nd^{3+} $^4G_{7/2}$, $^4G_{9/2}$, and $^2K_{13/2}$ levels are in the same spectral range (521 nm). Unfortunately the overlap of the Nd^{3+} $^4F_{3/2}\rightarrow{}^4I_{9/2}$ with the Er^{3+} $^4S_{3/2}\rightarrow{}^4I_{13/2}$ emission, prevents a definite statement for or against energy transfer. Previous work[33] on the effect of Nd^{3+}-Er^{3+} energy transfer on the $^4I_{13/2}$ lifetime indicates that the inclusion of 0.005 at. % Nd^{3+} should have no effect on this lifetime, i.e., no observable energy transfer. Our results suggest that Nd^{3+}-Er^{3+} energy transfer is negligible.

VI. CONCLUSIONS

The Judd-Ofelt theory has been used extensively to predict radiative rates of transitions for rare-earth ions in crystals, glasses, or solutions. In this paper we have investigated the reliability of the Judd-Ofelt predictions by extensive temperature-dependent-lifetime measurements. Room-temperature-lifetime measurements are found to be representative of the radiative rate only when the number of phonons required for the nonradiative transition is ten or greater. This investigation confirms the predictions of the Judd-Ofelt theory using measurements of *low-temperature* lifetimes. The differences between calculated and measured rates are within the established limits on the accuracy of the predicted rates ($\sim$10–25 %) (Refs. 25 and 32) or can be accounted for by multiphonon emission. The low-temperature value of the multiphonon-emission rate and the temperature dependence can be accounted for by the configuration-coordinate model of Huang and Rhys. This model predicted essentially the same values as those found with the often used "single-phonon model" up to room temperature. It was in better agreement with the data at higher temperatures. The method developed by Flaherty and DiBartolo[20] for the determination of radiative and nonradiative rates of Er^{3+} in MnF_2 was used for one level and found to agree with the Judd-Ofelt predicted rates, within the accuracy of the methods. The Flaherty-DiBartolo method was found to be very sensitive to the accuracy of the data used. It can only be applied with confidence to adjacent emitting states. Both conditions limit its applicability.

Our results indicate that the optical properties of Er^{3+}-doped fluorozirconate glass are similar to those for Er^{3+}-doped crystals. The emission lifetimes are very close to single exponential, even under broadband excitation. The absorption and emission bands are relatively narrow when compared to similar bands in oxide glasses. The observed multiphonon-emission rates of the $^4S_{3/2}$ and $^4F_{9/2}$ levels are lower, by over an order of magnitude, than the observed rates in germanate or tellurite glasses.[14,15,18] Research on the nonlinear refractive index and stimulated-emission cross section of ZBL:Nd also suggest the usefulness of these glasses as laser hosts.[28] More research on the thermal properties of these glasses is needed to ensure their usefulness for high-power laser applications, but in all other respects fluorozirconate glass and other, similar heavy-metal fluoride glasses, appear to be as good or better laser hosts than oxide glasses.

ACKNOWLEDGMENTS

The authors would like to thank R. C. Powell and M. J. Weber for many helpful discussions.

[1]M. Poulain, M. Poulain, J. Lucas, and P. Brun, Mater. Res. Bull. 10, 243 (1975).

[2]M. Poulain, M. Chanthanasinh, and J. Lucas, Mater. Res. Bull. 12, 151 (1977).

[3]M. G. Drexhage, C. T. Moynihan, and M. Saleh Boulos, Mater. Res. Bull. 15, 213 (1980).

[4]M. Robinson, R. C. Pastor, R. R. Turk, D. P. Devor, and R. Braustein, Mater. Res. Bull. 15, 735 (1980).

[5]M. G. Drexhage, B. Bendow, and C. T. Moynihan, Laser Focus 16, 62 (1980).
[6]G. H. Dieke, *Spectra and Energy Levels of Rare-Earth Ions in Crystals* (Interscience, New York, 1968).
[7]M. J. Weber, Phys. Rev. 157, 231 (1967).
[8]M. J. Weber, Phys. Rev. B 8, 47 (1973).
[9]G. M. Renfro, J. C. Windscheif, W. A. Sibley, and R. F. Belt, J. Lumin. 22, 51 (1980).
[10]M. D. Shinn, J. C. Windscheif, D. K. Sardar, and W. A. Sibley, Phys. Rev. B 26, 2371 (1982).
[11]B. R. Judd, Phys. Rev. 127, 750 (1962).
[12]G. S. Ofelt, J. Chem. Phys. 37, 511 (1962).
[13]W. F. Krupke, Phys. Rev. 145, 325 (1966).
[14]R. Reisfeld and Y. Eckstein, J. Non-Cryst. Solids 15, 125 (1974).
[15]R. Reisfeld, G. Katz, N. Spector, C. K. Jorgensen, C. Jacoboni, and R. DePape, J. Solid State Chem. 41, 253 (1982).
[16]W. T. Carnall, P. R. Fields, and K. Rajnak, J. Chem. Phys. 49, 4424 (1968).
[17]M. J. Weber, Phys. Rev. 157, 262 (1967).
[18]C. B. Layne, W. H. Lowdermilk, and M. J. Weber, Phys. Rev. B 16, 10 (1977).
[19]C. B. Layne and M. J. Weber, Phys. Rev. B 16, 3259 (1977).
[20]J. M. Flaherty and B. DiBartolo, J. Lumin. 8, 51 (1973).
[21]K. Huang and A. Rhys, Proc. R. Soc. London, Ser. A 204, 406 (1950).
[22]C. W. Struck and W. H. Fonger, J. Lumin. 10, 1 (1975).
[23]W. H. Fonger and C. W. Struck, J. Lumin. 17, 241 (1978).
[24]B. G. Wybourne, *Spectroscopic Properties of Rare Earths* (Interscience, New York, 1965).
[25]L. A. Riseberg and M. J. Weber, in *Progress in Optics,* edited by E. Wolf (Elsevier, New York, 1976), Vol. 14, p. 89.
[26]R. Reisfeld and Y. Eckstein, J. Chem. Phys. 63, 4001 (1975).
[27]L. A. Riseberg and H. W. Moos, Phys. Rev. 174, 429 (1968).
[28]J. Lucas, M. Chanthanasinh, M. Poulain, M. Poulain, P. Brun, and M. J. Weber, J. Non-Cryst. Solids 27, 273 (1978).
[29]M. G. Drexhage, C. T. Moynihan, M. Saleh Boulos, and K. P. Quinlan, in *Proceedings of the Conference on the Physics of Fiber Optics,* edited by B. Bendow and S. S. Mitra (American Ceramic Society, Columbus, 1981).
[30]B. Bendow, P. K. Banerjee, M. G. Drexhage, J. Goltmann, S. S. Mitra, and C. T. Moynihan, Comm. Amer. Ceram. Soc. 65, C8 (1982).
[31]M. V. Iverson and W. A. Sibley, Phys. Rev. B 21, 2522 (1980).
[32]L. A. Riseberg, W. B. Gandrud, and H. W. Moos, Phys. Rev. 159, 262 (1967).
[33]J. D. Edwards and J. N. Sandoe, J. Phys. D 7, 1078 (1974).